Dissociative recombination and vibrational excitation of CO^+: model calculations and comparison with experiment

2015 Plasma Sources Sci. Technol. 24 035005

(http://iopscience.iop.org/0963-0252/24/3/035005)

IOP Publishing Plasma Sources Science and Technology

Plasma Sources Sci. Technol. **24** (2015) 035005 (15pp) doi:10.1088/0963-0252/24/3/035005

Dissociative recombination and vibrational excitation of CO^+: model calculations and comparison with experiment

J Zs Mezei[1,2,3], R D Backodissa-Kiminou[1], D E Tudorache[1,4], V Morel[5], K Chakrabarti[1,6], O Motapon[7], O Dulieu[2], J Robert[2], W-Ü L Tchang-Brillet[8], A Bultel[5], X Urbain[9], J Tennyson[10], K Hassouni[11] and I F Schneider[1,2]

[1] LOMC CNRS-UMR-6294, Université du Havre, 76058 Le Havre, France
[2] Laboratoire Aimé Cotton CNRS-UPR-3321, Université Paris-Sud, F-91405 Orsay, France
[3] Institute of Nuclear Research of the Hungarian Academy of Sciences, PO Box 51, H-4001 Debrecen, Hungary
[4] Laboratoire EM2C, CNRS UPR288, École Centrale Paris, 92295 Châtenay-Malabry, France
[5] CORIA CNRS-UMR-6614, Université de Rouen, F-76801 Saint-Etienne du Rouvray, France
[6] Department of Mathematics, Scottish Church College, 1 and 3 Urquhart Sq., Kolkata 700 006, India
[7] Physics Department, University of Douala, PO Box 24157, Douala, Cameroon
[8] LERMA, Observatoire de Paris, Sorbonne Universités, UPMC Université Paris 06, CNRS-UMR 8112, F-92195 Meudon, France
[9] Institute of Condensed Matter and Nanosciences, PAMO—Louvain-la-Neuve, Belgium
[10] Department of Physics and Astronomy, University College London, London WC1E 6BT, UK
[11] Laboratoire des Sciences des Procédés et des Matériaux (LSPM), UPR3407 CNRS, Université Paris 13, 99 Avenue Jean Baptiste Clément, 93430 Villetaneuse, France

E-mail: ioan.schneider@univ-lehavre.fr

Received 23 December 2014, revised 11 February 2015
Accepted for publication 26 February 2015
Published 29 April 2015

Abstract

The latest molecular data—potential energy curves and Rydberg/valence interactions—characterizing the super-excited electronic states of CO are reviewed, in order to provide inputs for the study of their fragmentation dynamics. Starting from this input, the main paths and mechanisms for CO^+ dissociative recombination are analyzed; its cross sections are computed using a method based on multichannel quantum defect theory. Convoluted cross sections, giving both isotropic and anisotropic Maxwellian rate coefficients, are compared with merged-beam and storage-ring experimental results. The calculated cross sections underestimate the measured ones by a factor of two, but display a very similar resonant shape. These facts confirm the quality of our approach for the dynamics, and call for more accurate and more extensive molecular structure calculations.

Keywords: dissociative recombination, electron impact vibrational excitation, vibrationally excited, multichannel quantum defect theory

(Some figures may appear in colour only in the online journal)

1. Introduction

Carbon monoxide (CO) is the most abundant molecule detected in the interstellar medium after molecular hydrogen, and being heteronuclear, is much easier to detect in emissions. Its observation at long wavelengths, as in radio astronomy, is the source of much of the information obtained on different interstellar environments, from molecular clouds in which protostars form and irradiate the surrounding residual material, to the circumstellar disks that surround stars at the end of their lives and to the cometary gases. Its spectrum has been intensively studied in the astrophysical context, since its

large binding energy implies that many electronically excited states possess discrete line spectra; see Rosen *et al* (1998), Chakrabarti and Tennyson (2006, 2007), Eidelsberg *et al* (2012) and references therein. In all cases, under the influence of ultraviolet radiation produced during the stellar cycle, CO is the subject of a rich photochemistry, implying the formation of, among other species, its cation, CO^+.

CO^+ was the first molecular ion discovered outside of the Earth (Fowler 1909), and has been identified as a major constituent of dense interstellar molecular clouds (Roueff *et al* 2010). CO^+ also occurs in flames (Krupente and Weissman 1965, Seaton 1966, Mitchell and Hus 1985), and is expected to be very abundant in the plasmas formed by the hypersonic entry of spacecraft and comets into the Martian atmosphere (Park *et al* 1994, Bultel *et al* 2006). Cold plasmas containing a large number of molecules and molecular ions constitute a subject of rising scientific interest, involving more and more technological applications. CO^+ is the most important of such molecular ionic species, since it occurs in practically all air-assisted processes. Its dissociative recombination (DR) can be regarded as the main photochemical process of carbon loss from the Martian atmosphere (Fox 1999) and it is considered the major source of excited $C(^1D)$ atoms.

The kinetic description of all the above mentioned environments requires a good knowledge of the rate coefficients of the dominant reactions, including those between electrons and molecular ions. As for the CO^+ ions, their abundance is strongly affected by the DR:

$$CO^+(v_i^+) + e^- \rightarrow C + O, \tag{1}$$

but is also affected by other related competitive processes, such as the *inelastic* ($v_f^+ > v_i^+$) and *superelastic* ($v_f^+ < v_i^+$) *collisions* with electrons:

$$CO^+(v_i^+) + e^- \rightarrow CO^+(v_f^+) + e^-. \tag{2}$$

Here v_i^+ and v_f^+ stand for the initial and final vibrational quantum number of the target ion, and rotational structure was neglected.

The pioneering theoretical study of the DR rate coefficient made by Guberman (2007) shows that the dominant routes for the DR process are curves of the $^3\Pi$, $^1\Pi$ and $^1\Sigma^+$ symmetries. Guberman calculated the rate constants at 300 K to be 4.2×10^{-7} cm^3 s^{-1} for $^{12}C^{16}O^+$ and 2.9×10^{-7} cm^3 s^{-1} for $^{13}C^{16}O^+$. The most recent storage-ring experiments of Rosen *et al* (1998) gave a rate coefficient of 2.75×10^{-7} cm^3 s^{-1} for $^{13}C^{16}O^+$, which is in good agreement with the calculations of Guberman. The earlier afterglow experiments (Geoghegan *et al* 1991) for $^{12}C^{16}O^+$ gave a rate coefficient of 1.6×10^{-7} cm^3 s^{-1}, which does not agree with the theoretical calculations for $v_i^+ = 0$ and may indicate that a proportion of the CO^+ in that experiment was vibrationally excited.

Recently, a series of *ab initio* calculations for the CO states relevant to the DR (and of the couplings between them) have been performed by Chakrabarti and Tennyson (2006, 2007) using the R-matrix method. The data obtained make a new multichannel quantum defect theory (MQDT) investigation of the process over the whole energy range explored by the experiments (Mitchell and Hus 1985, Rosen *et al* 1998) possible.

The main goal of the present work is to evaluate the DR cross sections and the thermal rate using the previously mentioned *ab initio* data of Chakrabarti and Tennyson (2006, 2007). The paper is structured in the following way. Section 2 outlines the main ideas and steps of our MQDT approach. Section 3 presents the molecular data used in the calculation. The main results are given in section 4 and the paper ends with conclusions.

2. The MQDT-type approach to DR

The MQDT approach (Giusti-Suzor 1980, Seaton 1983, Greene and Jungen 1985, Jungen 1996) has been shown to be a powerful method for the evaluation of the cross sections of the DR process. Although it has been applied with great success to several diatomic systems like H_2^+ and its isotopologues (Giusti-Suzor *et al* 1983, Schneider *et al* 1991, Takagi 1993, Tanabe *et al* 1995, Schneider *et al* 1997, Amitay *et al* 1999), O_2^+ (Guberman and Giusti-Suzor 1991, Guberman 2000), NO^+ (Sun and Nakamura 1990, Vâlcu *et al* 1998, Schneider *et al* 2000a) and triatomics like H_3^+ (Schneider *et al* 2000b, Kokoouline *et al* 2001, Kokoouline and Greene 2003), its application to vibrational transitions, mainly to superelastic collisions for NO^+, is relatively recent (Ngassam *et al* 2003a, Motapon *et al* 2006).

We aim to describe the sensitivity of the reactive electron–cation collisions to the *vibrational* levels involved. At least to a first approximation, rotational effects are known to be negligible for CO^+ (Vâlcu *et al* 1998). The reasons for this rely on the weak Rydberg–valence interaction responsible for the indirect process: since the rotational structures and interactions play roles especially within the indirect mechanism (due to its resonant character), the weakness of this latter process implies that the rotational effects—if of any relevance—can be roughly restricted to the existence of the centrifugal barrier, due to the rotational excitation. But even in this latter context, rotation does not matter very much, since the target ion and the neutral are *equally* excited and, consequently, the Franck–Condon overlaps (direct processes) do not change significantly with respect to those occurring for the case of rotationally ground states. However, this does not mean that the electron-impact rotational excitation is negligible (Faure and Tennyson 2001).

The theoretical summary given below is limited to an account of the vibrational structure and coupling, illustrated mainly for DR. However, the reader should keep in mind that the other competitive reactions—such as the superelastic collisions (SECs; $v_i^+ > v_f^+$ in equation (2)), elastic collisions (ECs; $v_i^+ = v_f^+$) and inelastic collisions (ICs; $v_i^+ < v_f^+$)—also occur and can display quite similar features.

The DR can take place following two mechanisms:

(a) the *direct* process where the capture takes place into a dissociative state of the neutral system (CO^{**}):

$$CO^+(v_i^+) + e^- \rightarrow CO^{**} \rightarrow C + O; \tag{3}$$

(b) the *indirect* process where the capture occurs via a Rydberg state of the molecule CO^* which is predissociated by the CO^{**} state:

$$CO^+(v_i^+) + e^- \rightarrow CO^* \rightarrow CO^{**} \rightarrow C + O. \quad (4)$$

We note here that we follow the standard nomenclature in this work, namely CO^{**} and CO^* represent the doubly excited and singly excited states of CO respectively. In both of these processes, autoionization is in competition with the predissociation and leads, through the reaction (2), to SECs, ECs or ICs. The MQDT treatment of DR involves ionization channels (describing the electron–ion scattering) and dissociation channels (describing the atom–atom scattering). Each ionization channel consists of a Rydberg series of excited states, extrapolated above the continuum threshold—a vibrational level v^+ of the molecular ion. A channel is considered *open* if its corresponding threshold is situated *below* the total energy of the system, and *closed* in the opposite case. In the present work we have $N^+ = N$ (where N and N^+ stand for the rotational quantum number of the neutral and ion, respectively), and as for the dissociative channels, only open channels are used.

The present MQDT approach is based on a description of molecular states in which only part of the electronic Hamiltonian is diagonalized, within subspaces of electronic states with similar natures. Moreover, we use a quasi-diabatic representation of molecular states (Sidis and Lefebvre-Brion 1971) to cope with problems due to the avoided crossings of the potential energy curves. The short-range electronic interactions between states of different subspaces are then represented in terms of an electronic coupling operator $\boldsymbol{\mathcal{V}}$ given by

$$\mathcal{V}^{\Lambda}_{d_j,lv}(E',E) = \left\langle \chi^{\Lambda}_{d_j}(R) | V^{\Lambda}_{d_j,l}(R) | \chi^{\Lambda}_{v}(R) \right\rangle, \quad (5)$$

which couples the ionization channels (labeled with lv) to the dissociative channels (labeled with d_j). Starting from $\boldsymbol{\mathcal{V}}$, one can build the short-range reaction matrix $\boldsymbol{\mathcal{K}}$, which is a solution of the Lippmann–Schwinger integro-differential equation:

$$\boldsymbol{\mathcal{K}} = \boldsymbol{\mathcal{V}} + \boldsymbol{\mathcal{V}} \frac{1}{E - \boldsymbol{H_0}} \boldsymbol{\mathcal{K}}, \quad (6)$$

$\boldsymbol{H_0}$ being the zeroth-order Hamiltonian associated with the molecular system, i.e. the Hamiltonian operator excluding the interaction potential $\boldsymbol{\mathcal{V}}$. The short-range effects are valid in the region of small electron–ion and nuclei–nuclei distances, namely in the 'A-region' (Jungen and Atabek 1977) where the Born–Oppenheimer representation is appropriate for the description of the colliding system. Here, the energy dependence of the electronic couplings can be neglected. In the case of weak coupling, a perturbative solution of equation (6) can be obtained. This solution has been proved to be exact to second order in the case of energy-independent electronic couplings (Ngassam *et al* 2003b). In the external zone, the 'B-region' (Jungen and Atabek 1977) represented by large electron–core distances, the Born–Oppenheimer model is no longer valid for the ionization channels and a close coupling representation in terms of 'a molecular ion plus an electron' is more appropriate. This corresponds to a frame transformation defined by the projection coefficients:

$$\mathcal{C}_{lv^+,\Lambda\alpha} = \sum_v U^{\Lambda}_{lv,\alpha} \langle \chi_{v^+} | \cos(\pi\mu_l^{\Lambda}(R) + \eta^{\Lambda}_{\alpha}) | \chi^{\Lambda}_{v} \rangle, \quad (7)$$

$$\mathcal{C}_{d_j,\Lambda\alpha} = U^{\Lambda}_{d_j\alpha} \cos\eta^{\Lambda}_{\alpha}, \quad (8)$$

$$\mathcal{S}_{lv^+,\Lambda\alpha} = \sum_v U^{\Lambda}_{lv,\alpha} \langle \chi_{v^+} | \sin(\pi\mu_l^{\Lambda}(R) + \eta^{\Lambda}_{\alpha}) | \chi^{\Lambda}_{v} \rangle, \quad (9)$$

$$\mathcal{S}_{d_j,\Lambda\alpha} = U^{\Lambda}_{d_j\alpha} \sin\eta^{\Lambda}_{\alpha}. \quad (10)$$

Here, χ_{v^+} is the vibrational wavefunction of the molecular ion, and χ^{Λ}_{v} is a vibrational wavefunction adapted to the interaction region (A-region). The index α denotes the eigenchannels built through the *diagonalization* of the reaction matrix $\boldsymbol{\mathcal{K}}$ in equation (6), and $U^{\Lambda}_{lv,\alpha}$ and η^{Λ}_{α} are related to the corresponding eigenvectors and eigenvalues, while Λ refers to the electronic symmetry of the neutral species ($^1\Sigma^+$, $^1\Pi$, and $^3\Pi$ in the present study).

The projection coefficients shown in (7)–(10) include the two kinds of couplings controlling the process: the *electronic* coupling, expressed by the elements of the matrices $\boldsymbol{U}$ and $\boldsymbol{\eta}$, and the *non-adiabatic* coupling between the ionization channels, expressed by the matrix elements involving the quantum defect μ_l^{Λ}. This latter interaction is favored by the variation of the quantum defect with the internuclear distance R. The matrices $\boldsymbol{\mathcal{C}}$ and $\boldsymbol{\mathcal{S}}$ with the elements given by (7)–(10) are the building blocks of the 'generalized' scattering matrix $\boldsymbol{X}$:

$$\boldsymbol{X} = \frac{\boldsymbol{\mathcal{C}} + i\boldsymbol{\mathcal{S}}}{\boldsymbol{\mathcal{C}} - i\boldsymbol{\mathcal{S}}}, \quad (11)$$

whereas the 'proper' scattering matrix, restricted to the open channels, is given by Seaton (1983)

$$\boldsymbol{S} = \boldsymbol{X}_{oo} - \boldsymbol{X}_{oc} \frac{1}{\boldsymbol{X}_{cc} - \exp(-i\,2\pi\boldsymbol{\nu})} \boldsymbol{X}_{co}. \quad (12)$$

More precisely, the physical S-matrix is obtained from the 2×2 submatrices of $\boldsymbol{X}$ involving the open (o) and closed (c) channels, and from the diagonal matrix $\boldsymbol{\nu}$ containing the effective quantum numbers $\nu_{v^+} = [2(E_{v^+} - E)]^{-1/2}$ (in atomic units) associated with each vibrational threshold E_{v^+} of the ion situated above the current energy E. For a molecular ion initially in vibrational level v_i^+ and recombining with an electron of energy ϵ, the cross section for capture into *all* of the dissociative states d_j of the same symmetry Λ is given by

$$\sigma^{\Lambda}_{\text{diss}\leftarrow v_i^+} = \frac{\pi\rho^{\Lambda}}{4\epsilon} \sum_j \sum_l |S^{\Lambda}_{d_j \leftarrow lv_i^+}|^2, \quad (13)$$

where ρ^{Λ} is the ratio of the multiplicities of the neutral system and the ion. One has to perform the MQDT calculation for each group of dissociative states of symmetry Λ, and the sum over the resulting cross sections is the total DR cross section:

$$\sigma_{\text{diss}\leftarrow v_i^+} = \sum_{\Lambda} \sigma^{\Lambda}_{\text{diss}\leftarrow v_i^+}. \quad (14)$$

In a similar way, the cross section for a vibrational transition of a molecular ion from the initial level v_i^+ to the final level v_f^+ is (excitation and/or de-excitation)

$$\sigma^{\Lambda}_{v_f^+\leftarrow v_i^+} = \frac{\pi}{4}\frac{\rho^{\Lambda}}{\varepsilon}\sum_{l,l'} |S^{\Lambda}_{l'v_f^+\leftarrow lv_i^+}|^2, \tag{15}$$

while the total cross section for this vibrational transition reads

$$\sigma_{v_f^+\leftarrow v_i^+} = \sum_{\Lambda}\sigma^{\Lambda}_{v_f^+\leftarrow v_i^+}. \tag{16}$$

3. Molecular data

3.1. Ab initio R-matrix calculations

The earliest attempts to compute excited states of CO relevant for the dissociative recombination and their autoionization widths go back to 1996 (Tennyson 1996a, 1996b), but they were restricted to a single geometry.

Ten years later, two of us (Chakrabarti and Tennyson 2006, Chakrabarti and Tennyson 2007) performed a much more detailed R-matrix calculation for a series of fixed geometries. These calculations used up to 14 lowest CO^+ states in a close coupling expansion where each of these states was represented using a valence complete active space configuration interaction expansion. The calculations were repeated for 10 different internuclear distances in the range of 1.5 a_0–3.5 a_0. Moreover, Chakrabarti and Tennyson (2007) computed positions and widths for a number of dissociative states, which appear as resonances in the R-matrix scattering calculations, as a function of the geometry. In particular, resonance states of electronic symmetry $^1\Sigma^+$, $^1\Pi$ and $^3\Pi$ have been used in the present work, as the other symmetries are only very weakly coupled.

Although the R-matrix resonance calculations (Chakrabarti and Tennyson 2007) for the CO molecule have not been subjected to comparisons and calibrations against all available spectroscopic data, some Rydberg states previously calculated by Tennyson (1996a) and Chakrabarti and Tennyson (2006) were. It was found that these Rydberg states are placed higher than the observed values, which is consistent with the variational nature of the R-matrix calculations. As a consequence, for low ℓ values, the estimated quantum defects were uniformly lower by about 0.07 as compared to the available experimental data; see for example tables 4 and 5 in Chakrabarti and Tennyson (2006). The geometry-dependent study on CO also showed that the quantum defects depend weakly on the geometry except when the adiabatic curves are perturbed by an avoided crossing. This approach was successfully used by Schneider *et al* (2000a) to give greatly improved results for DR of NO^+.

3.2. Modeling of the dissociative curves

The DR cross section is extremely sensitive to the positions of the potential energy curves (PECs) of the neutral dissociative states with respect to that of the target ion. More specifically, a slight change of the point of crossing of the PEC of a neutral dissociative state with that of the ion ground state can lead to a significant change in the predicted DR cross section. The magnitude of this change is roughly proportional to the square of the Franck–Condon-type integral appearing in equation (5). This is an important issue here, as we use the approximate PECs of the dissociative states above the ion ground state produced by R-matrix calculations (Chakrabarti and Tennyson 2006, Chakrabarti and Tennyson 2007). Indeed, for example, the crossing point of the lowest relevant $^1\Sigma^+$ state was found to be at higher energy and at larger internuclear distance than those obtained previously using a de-perturbation procedure (Tchang-Brillet *et al* 1992) or *ab initio* quantum chemistry computations (Guberman 2007). Moreover, recent calculations (Lefebvre-Brion and Lewis 2007, Vázquez *et al* 2009, Lefebvre-Brion *et al* 2010) give PECs for the *lowest* neutral states relevant for DR that only partially agree with those from the other calculations mentioned above.

All of the available lower dissociative neutral states for the $^1\Sigma^+$ symmetry are shown in figure 1, where we have presented the PECs relevant for the present study. The zero of energy was chosen to be the lowest vibrational level of the ground electronic state of the molecular ion. At the same time the MQDT calculation requires, besides the dissociative curves, the couplings between the ion ground state and the neutral dissociative states. The R-matrix calculations of Chakrabarti and Tennyson (2007) systematically provide autoionization widths for a large number of states which contain information about the required couplings. Such comprehensive data on couplings are not available from any other source. Thus we use their data in our dynamical study on DR but correct the PECs when this is needed. In this way we undertake a semi-empirical calculation.

The dissociative (valence) states produce numerous avoided crossings when crossing the series of Rydberg states. On turning to the diabatic representation, these avoided crossings become 'true' crossings essential for the *indirect* process. A quasi-diabatic PEC may be constructed by smoothly connecting the resonant states obtained by scattering calculations to the asymptotic adiabatic states. A more detailed inspection of the available material, both diabatic and adiabatic, confirms the quality of the diabatic states obtained by Guberman (2007), justifying their use in the construction of quasi-diabatic PECs by matching them in the relevant range of internuclear distances. As a general rule, we apply a slight shift to the R-matrix PECs only if it is necessary in order to match them with the diabatic curves of Guberman (2007). This is clearly the case for the first state of $^1\Sigma^+$ symmetry; see figure 1. No such behavior is visible for the second dissociative PEC, but we apply the same shift in quantum defect as we applied to connect the first state to its quasi-diabatic counterpart. Correlation with the proper asymptotic limits follows both the Wigner and Witmer (1928) rules and the adiabatic curves of Vázquez *et al* (2009), where they are available. In our model, we construct the lowest dissociative states as a function of the internuclear distance on the basis of a physically reasonable compromise between the available valence curves coming from all of the above cited authors. As an example, consider the lowest state of $^1\Sigma^+$ symmetry. At the smaller internuclear distances, our quasi-diabatic PEC follows the R-matrix points of

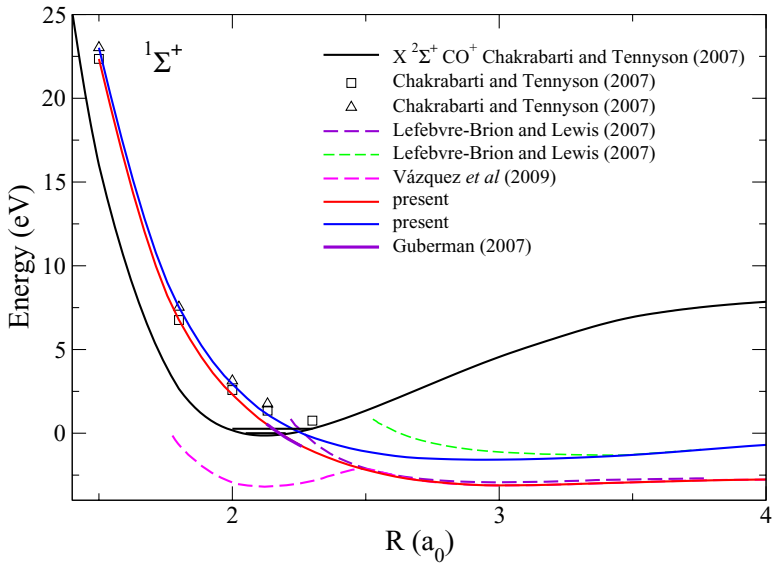

Figure 1. Electronic states relevant for dissociative recombination with $^1\Sigma^+$ total symmetry. The ion ground state is shown in black; □, Δ show the R-matrix data (Chakrabarti and Tennyson 2007) for the lowest two CO^{**} states. The two continuous colored curves crossing the ion are the dissociative states obtained as outlined in section 3.2. The curves indicated in the legends refer to the curves from Guberman (2007), Lefebure-Brion and Lewis (2007) and Vázquez *et al* (2009).

Chakrabarti and Tennyson (2007). At larger internuclear distances we shift the R-matrix dissociative curve progressively in order to match them with those of Guberman (2007). This curve is used until its crosses the PEC of the molecular ion, and beyond, followed by a smooth connection to the lowest *diabatic* PEC of Lefebvre-Brion and Lewis (2007), which agrees very well with the asymptotic behavior of the lowest *adiabatic* potential energy curves of Vázquez at large internuclear distances. The dissociative curves constructed in this way will agree well with the PEC used by Guberman. A similar procedure is followed for all of the other excited states with different symmetries.

As regards the highest R-matrix dissociative PECs, we believe that they are robust, since the inherent errors in the R-matrix calculations decrease significantly within the degree of excitation. Finally, figure 2 shows the ion ground state and vibrational levels, and the adjusted dissociative curves used in the present calculations and their corresponding autoionization widths coming from the R-matrix computations.

4. Evaluation of the cross section using the MQDT-type approach

4.1. Mechanisms and couplings

Using the set of molecular data (PECs and electronic couplings) determined as described in the previous section, we performed a series of MQDT calculations of the DR cross section, assuming the molecular ion to be initially in its electronic ground state ($X^2\Sigma^+$, $v_i^+ = 0, 1, 2$) and neglecting rotational and spin–orbit effects. The calculations were performed for the states with total symmetry of $^1\Sigma^+$, $^1\Pi$ and $^3\Pi$, while the numbers of dissociative states considered for each symmetry are indicated in figure 2.

We consider incident electron energies from 0.01 meV up to 3 eV. Since the dissociation energy of $CO^+(X^2\Sigma^+)$ is about 8.5 eV, the majority of the 53 vibrational levels of the ion lie above the total energy of the CO^+ +e system. These levels are associated with closed ionization channels, as defined in section 2, responsible for temporary resonant capture into Rydberg states. As the energy increases, more and more ionization channels become open, which can result in autoionization, leading to competitive processes like ICs and SECs, decreasing the flux of DR.

The direct electronic couplings between ionization and dissociation channels—equation (5)—have been extracted from the autoionization widths of the valence states (Chakrabarti and Tennyson 2007).

Since a highly accurate solution of the Lippman–Schwinger system of integral equation (6) is difficult to obtain (Pichl *et al* 2000, Takagi 2000), we take advantage of the fact that the couplings (among the ionization and dissociation channels) involved are small and a perturbative solution is acceptable. Following the main ideas of the earlier studies (Guberman and Giusti-Suzor 1991, Schneider *et al* 1991), we adopt a second-order perturbative expansion, which accounts for all of the basic mechanisms involved in DR, including the indirect electronic interaction between the ionization channels.

The non-adiabatic couplings between the ionization channels rely (see equations (7) and (8)) on the R-dependences of the quantum defects, which have been evaluated using the *ab initio* calculations described in section 3.1.

For each dissociative channel available, we have considered the interaction with the most relevant series of Rydberg states, namely for $^1\Sigma^+$ symmetry the lowest four partial waves (s, p, d and f) were considered, while for the $^1\Pi$ and $^3\Pi$ symmetries only the lowest three (s, p, d) have been used. For the sake of simplicity, figure 2 shows the so-called global

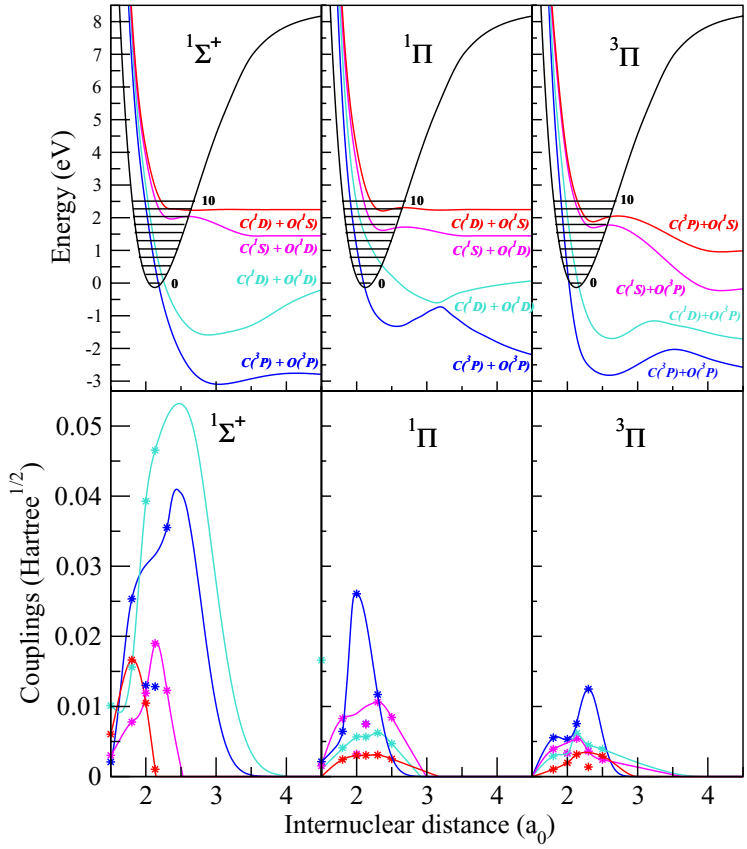

Figure 2. The dissociative curves and couplings relevant for CO^+ dissociative recombination for the symmetries indicated in each figure. Top panel: the adjusted potential energy curves (see section 3), the ion ground state and the first ten vibrational levels are represented in black. Bottom panel: couplings between the valence dissociative states and the ionization continua.

couplings which were constructed using the autoionization widths of Chakrabarti and Tennyson (2006, 2007), namely $V^{\Lambda}_{d_j} = ((\sum_l \Gamma^{\Lambda}_{d_j,l})/2\pi)^{1/2}$.

According to equation (12), the interference between the direct process (involving open channels exclusively and described by the first term: $\boldsymbol{X_{oo}}$) and the indirect one (involving closed as well as open channels and accounted for by the second term) results in the total process.

The role of the direct and indirect mechanisms in the DR process can be seen in figure 3. The full colored lines show the total cross sections for the different symmetries used in the calculations, while dashed lines of the same color represent the cross sections given by the direct process only. As one could expect from the magnitude of the valence–Rydberg couplings (see figure 2), a strong dependence on the states and interactions can be observed. The majority of the cross section is given by the $^1\Pi$ and $^1\Sigma^+$ symmetries, while the $^3\Pi^+$ symmetry contributes only a small part. Moreover, for both states with Π symmetry, the indirect process plays a minor role for this ion; the magnitude of the total cross section is given by the direct process, and the indirect one is responsible for the resonance structures. This is most striking for the $^1\Pi$ symmetry, where the total and direct-only cross sections lie on top of each other. The importance of the indirect mechanism is relevant for the $^1\Sigma$ symmetry, where due to the *destructive* interference between the direct and indirect processes the total cross section is lowered by almost an order of magnitude compared to the direct one, at certain collision energies. The indirect processes give rise to broad resonance structures in the range of the collision energy of the present study. Even though the indirect process globally plays a minor role, evaluating its effect gives increased insight into the recombination mechanism.

The levels of importance of the different dissociation paths in our calculation are summarized in table 1. Our calculated final state distributions are compared with the experimental values of Rosen *et al* (1998) for four relative collision (detuning) energies. For zero collision energy the statistical error was evaluated to be about 5%, while for higher energy values, due to the poor statistics, it is around 30%.

The dominant dissociation pathway for the DR of the CO^+ is the one which correlates with the $C(^3P) + O(^3P)$ atomic limits. Table 1 shows a qualitative agreement between the calculated and the measured final state distributions. The agreement is good at low collision energies. At higher energies, the two sets of data disagree, mainly due to the increased experimental statistical errors and the fact that our model lacks a dissociating pathway correlating with the $C(^3P) + O(^1D)$ atomic limits.

5. Results and discussion

The DR cross sections corresponding to the three symmetries contributing to the process ($^1\Sigma^+$, $^1\Pi$ and $^3\Pi$), summed

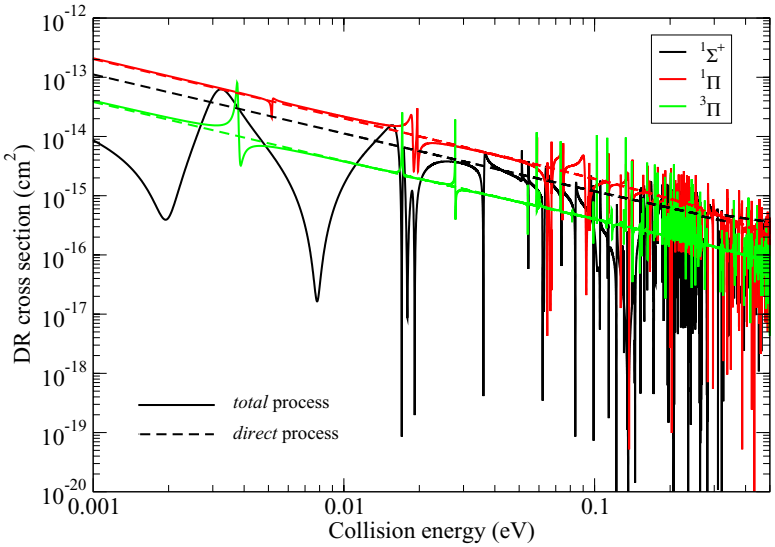

Figure 3. Cross sections for the direct (dashed lines) and the total (direct plus indirect) processes (continuous lines), for a vibrationally relaxed target in electronic states with $^1\Sigma^+$ (black), $^1\Pi$ (red) and $^3\Pi$ (blue) symmetries.

Table 1. The calculated final state distributions and their comparison with the experimental values for four relative collision (detuning) energies.

Dissociation path	Energy (eV)							
	10^{-5}		0.4		1		1.5	
	Calc. (%)	Exp.[a] (%)	Calc. (%)	Exp. (%)	Calc. (%)	Exp. (%)	Calc. (%)	Exp. (%)
$C(^3P) + O(^3P)$	86.56	76.1	80.85	53	43.25	39	50.93	38
$C(^3P) + O(^1D)$	—	9.4	—	8	—	15	—	11
$C(^1D) + O(^3P)$	13.41	14.5	19.15	34	9.61	35	4.50	35
$C(^1S) + O(^3P)$		0.0			$<10^{-5}$	5	$<10^{-2}$	5
$C(^1D) + O(^1D)$				5	47.14	6	44.56	11
$C(^3P) + O(^1S)$							$\sim 10^{-11}$	
$C(^1S) + O(^1D)$		—		—		—	$\sim 10^{-7}$	—

[a] (Rosen *et al* 1998).

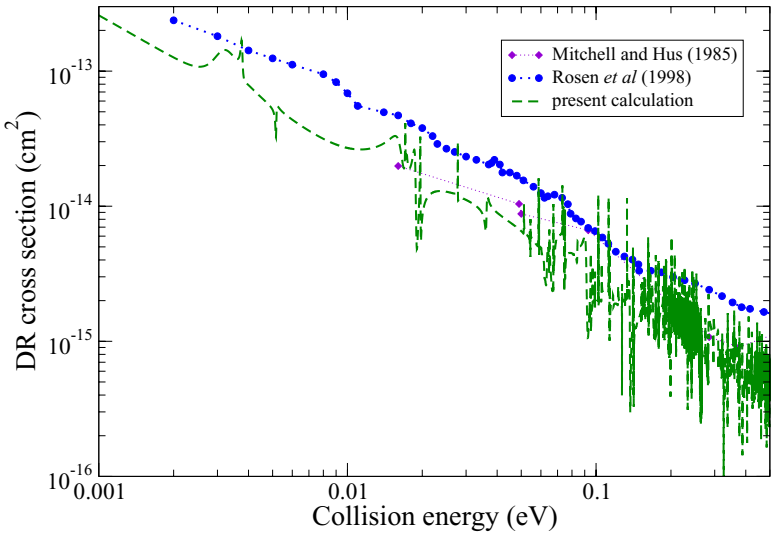

Figure 4. Cross sections for the total (direct plus indirect) DR process for a vibrationally relaxed target including the summed contributions of the states with $^1\Sigma^+$, $^1\Pi$ and $^3\Pi$ symmetry. The experimental results of Mitchell and Hus (1985) are shown with a dotted line with full violet diamonds, while those of Rosen *et al* (1998) are shown with a dotted line with full blue circles.

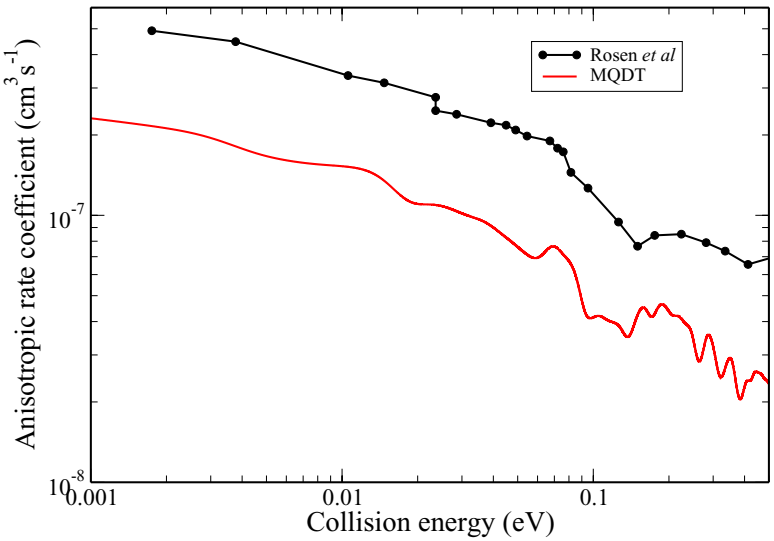

Figure 5. Anisotropic rate coefficients for a vibrationally relaxed target. Experimental results (Rosen *et al* 1998) are in given in black with filled circles. Our theoretical results, for all symmetries considered here, are shown in red.

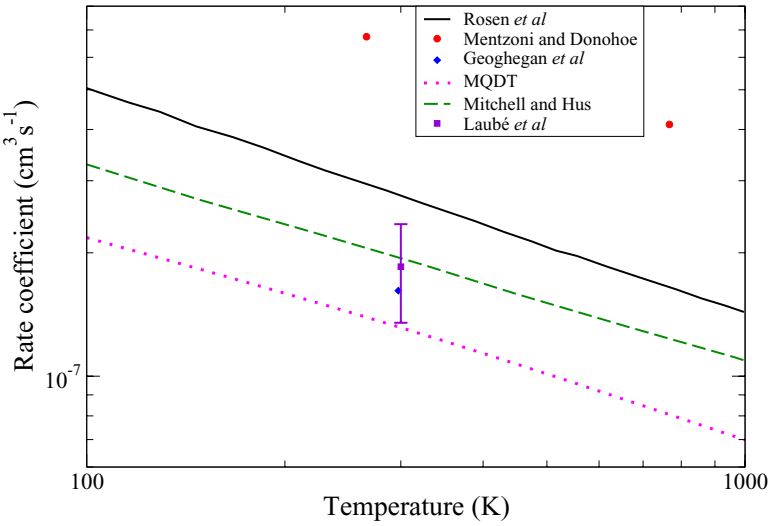

Figure 6. Isotropic rate coefficients for a vibrationally relaxed target. Our theoretical results, for all symmetries considered here, are represented by magenta dotted lines. The experimental results are shown as follows: Mitchell and Hus (1985), green dashed line; Rosen *et al* (1998), black solid line; Geoghegan *et al* (1991), blue diamonds; Mentzoni and Donohoe (1968), red circles; and Laubé *et al* (1998), violet squares.

according to equation (14), are shown in figure 4. The calculations have been performed for the $^{12}C^{16}O^+$ isotopologue of the cation. The total cross section is characterized by resonance structures, superimposed on a smooth background (direct process only). The strong interaction between the closed channels, associated with higher vibrational ion levels and the current dissociative states, contaminates, via non-adiabatic or indirect electronic coupling, the direct interaction between the entrance and the dissociative channels. This results in a stronger capture probability, and consequently a higher DR cross section, which leads to the rich resonance structures observed in the total cross section. The direct DR cross section is proportional to the square of the Franck–Condon overlap, of the type seen in equation (5), between the vibrational wavefunctions of the ion and the dissociation state of the neutral. The favorable crossings at lower collision energies of the dissociation states correlating with the C(^{3}P) + O(^{3}P) and C(^{1}D) + O(^{1}D) atomic limits (blue and cyan curves in figure 2) with the ionic ground state (black curve in the same figure) and the significant couplings to the entrance channel are responsible for the large contribution from the direct DR cross sections to all three of the symmetries used in the calculations. This is the smooth background cross section on which the contribution from the indirect process is superimposed, resulting in the total cross section shown in figure 4. The closed ionization channels are those responsible for the temporary capture into the Rydberg states and consequently into the indirect mechanism. There are an increasing number of resonance states of all symmetries at higher energies, and some or all of these can participate in the DR process via the channel mixing mechanism.

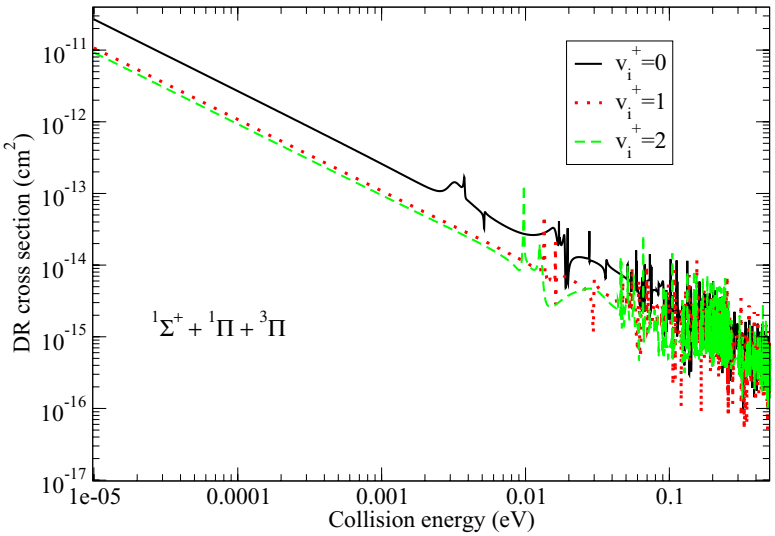

Figure 7. Total DR cross sections for different initial vibrational levels of the ion, for all of the symmetries considered. Black continuous lines stand for $v_i^+ = 0$, while the red dotted and green dashed lines stand for $v_i^+ = 1$ and 2, respectively.

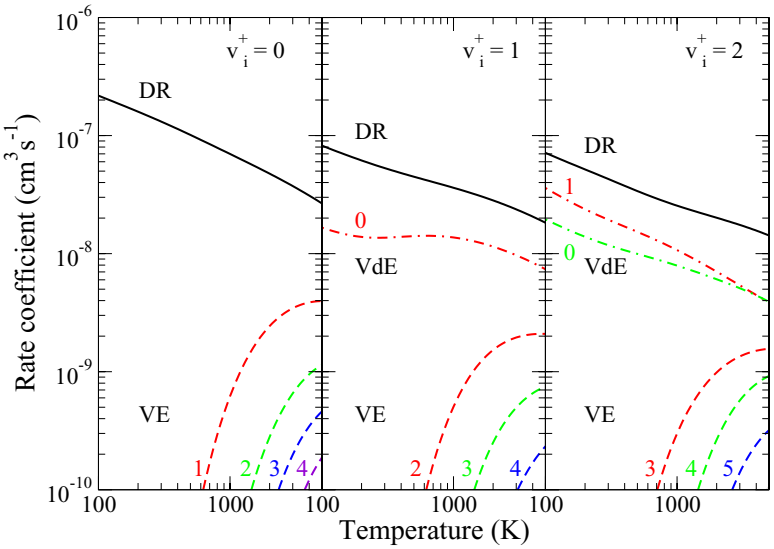

Figure 8. DR and state-to-state VE and VdE isotropic rate coefficients of CO^+ in its ground electronic state, v_i^+ standing for the vibrational quantum number of the target ion. Curves of the same color show the rate coefficients for the vibrational (de-)excitations corresponding to the same $|\Delta v| = |v_f^+ - v_i^+|$; $v_f > v_i$ for the VE and $v_f < v_i$ for the VdE global rate coefficients. The final vibrational quantum numbers of the ion are indicated for these processes.

The role of each dissociation channel depends on the energy of the incident electron. At higher collision energies, when the other two dissociation channels become open (magenta and red curves in figure 2), due to their less favorable crossings with the ionic ground state, the indirect process gains importance, leading to the resonance structures in the total cross section. We have included all of the contributions of the dissociative channels in our calculations.

In view of the comparison with the storage-ring measurements, we have convoluted our MQDT cross sections with the anisotropic Maxwell velocity distribution function for the electrons. The transverse and longitudinal temperatures are $K_B T_\perp = 1$ meV and $K_B T_\parallel = 10$ meV, respectively. The calculated anisotropic rate coefficient (magenta) and the measured one (green) (Rosen *et al* 1998) are shown in figure 5. The overall agreement with experimental values is good; our calculated rate coefficient reproduces perfectly the trends of the experimental curves, underestimating them on average by a factor of 2.

We have evaluated in addition to the anisotropic rate coefficients, starting from the computed cross section, the Maxwell isotropic rate coefficient as well, for a broad range of electronic temperatures, relevant especially for cold non-equilibrium plasmas. The rate for $v_i^+ = 0$ is displayed in figure 6; its thermal value (300 K) is in excellent agreement with the measured values obtained in a merged beam by Mitchell and Hus (1985) and Laubé *et al* (1998), as well as storage-ring-based (Rosen *et al* 1998) collision experiments. The rate coefficients of Mentzoni and Donohoe (1968) presented as red circles in the figure are higher than the other

Table 2. Parameters used in equation (17) to represent the DR rate coefficients of CO^+.

v	A_v	α_v	$B_v(1)$	$B_v(2)$	$B_v(3)$	$B_v(4)$	$B_v(5)$	$B_v(6)$	$B_v(7)$
0	$0.281\,949\,503 \times 10^{-4}$	$-0.802\,579\,890 \times 10^{0}$	$0.710\,130\,957 \times 10^{3}$	$-0.698\,308\,895 \times 10^{6}$	$0.335\,177\,615 \times 10^{9}$	$-0.850\,620\,477 \times 10^{11}$	$0.117\,104\,453 \times 10^{14}$	$-0.826\,280\,436 \times 10^{15}$	$0.233\,919\,918 \times 10^{17}$
1	$0.715\,701\,893 \times 10^{-5}$	$-0.682\,706\,983 \times 10^{0}$	$0.843\,520\,677 \times 10^{3}$	$-0.713\,971\,932 \times 10^{6}$	$0.300\,490\,272 \times 10^{9}$	$-0.703\,053\,442 \times 10^{11}$	$0.920\,945\,293 \times 10^{13}$	$-0.629\,626\,035 \times 10^{15}$	$0.174\,554\,736 \times 10^{17}$
2	$0.158\,116\,294 \times 10^{-5}$	$-0.537\,454\,517 \times 10^{0}$	$0.740\,102\,970 \times 10^{3}$	$-0.910\,764\,930 \times 10^{6}$	$0.460\,910\,057 \times 10^{9}$	$-0.118\,698\,360 \times 10^{12}$	$0.163\,967\,837 \times 10^{14}$	$-0.115\,670\,469 \times 10^{16}$	$0.327\,041\,619 \times 10^{17}$

Table 3. Parameters used in equation (18) to represent the VE rate coefficients of CO^+ ($v' = 0$).

$v' \to v''$	$T_{\min}$ (K)	$A_{v' \to v''}$	$\alpha_{v' \to v''}$	$B_{v' \to v''}(1)$	$B_{v' \to v''}(2)$	$B_{v' \to v''}(3)$	$B_{v' \to v''}(4)$	$B_{v' \to v''}(5)$	$B_{v' \to v''}(6)$	$B_{v' \to v''}(7)$
$0 \to 1$	100	$0.641\,552\,103 \times 10^{-5}$	$-0.771\,371\,374 \times 10^{0}$	$0.414\,475\,403 \times 10^{4}$	$-0.555\,697\,606 \times 10^{6}$	$0.177\,113\,555 \times 10^{9}$	$-0.379\,319\,033 \times 10^{11}$	$0.499\,340\,108 \times 10^{13}$	$-0.353\,310\,994 \times 10^{15}$	$0.101\,763\,661 \times 10^{17}$
$0 \to 2$	200	$0.748\,711\,072 \times 10^{-5}$	$-0.848\,613\,994 \times 10^{0}$	$0.808\,028\,559 \times 10^{4}$	$-0.314\,102\,151 \times 10^{7}$	$0.267\,788\,469 \times 10^{10}$	$-0.125\,332\,604 \times 10^{13}$	$0.323\,013\,435 \times 10^{15}$	$-0.429\,933\,877 \times 10^{17}$	$0.230\,779\,467 \times 10^{19}$
$0 \to 3$	250	$0.653\,782\,258 \times 10^{-5}$	$-0.889\,871\,881 \times 10^{0}$	$0.100\,400\,799 \times 10^{5}$	$-0.153\,427\,057 \times 10^{7}$	$0.166\,204\,703 \times 10^{10}$	$-0.968\,343\,280 \times 10^{12}$	$0.307\,963\,790 \times 10^{15}$	$-0.505\,267\,521 \times 10^{17}$	$0.334\,692\,067 \times 10^{19}$
$0 \to 4$	300	$0.410\,991\,022 \times 10^{-4}$	$-0.111\,309\,015 \times 10^{1}$	$0.144\,578\,277 \times 10^{5}$	$-0.425\,122\,442 \times 10^{7}$	$0.457\,572\,230 \times 10^{10}$	$-0.279\,947\,663 \times 10^{13}$	$0.974\,452\,298 \times 10^{15}$	$-0.180\,068\,315 \times 10^{18}$	$0.137\,000\,155 \times 10^{20}$
$0 \to 5$	350	$0.673\,816\,604 \times 10^{-4}$	$-0.121\,225\,593 \times 10^{1}$	$0.186\,129\,714 \times 10^{5}$	$-0.751\,669\,966 \times 10^{7}$	$0.865\,504\,846 \times 10^{10}$	$-0.581\,314\,625 \times 10^{13}$	$0.227\,948\,002 \times 10^{16}$	$-0.482\,391\,689 \times 10^{18}$	$0.424\,701\,037 \times 10^{20}$
$0 \to 6$	400	$0.678\,304\,142 \times 10^{-4}$	$-0.126\,655\,170 \times 10^{1}$	$0.216\,968\,564 \times 10^{5}$	$-0.932\,715\,458 \times 10^{7}$	$0.125\,788\,319 \times 10^{11}$	$-0.980\,812\,594 \times 10^{13}$	$0.440\,562\,841 \times 10^{16}$	$-0.105\,632\,400 \times 10^{19}$	$0.104\,556\,888 \times 10^{21}$
$0 \to 7$	450	$0.935\,214\,058 \times 10^{-4}$	$-0.135\,011\,215 \times 10^{1}$	$0.242\,759\,946 \times 10^{5}$	$-0.866\,103\,794 \times 10^{7}$	$0.131\,034\,124 \times 10^{11}$	$-0.117\,137\,348 \times 10^{14}$	$0.603\,374\,022 \times 10^{16}$	$-0.165\,375\,862 \times 10^{19}$	$0.186\,623\,905 \times 10^{21}$
$0 \to 8$	500	$0.127\,223\,673 \times 10^{-3}$	$-0.143\,309\,661 \times 10^{1}$	$0.268\,650\,737 \times 10^{5}$	$-0.655\,138\,124 \times 10^{7}$	$0.888\,503\,051 \times 10^{10}$	$-0.729\,741\,009 \times 10^{13}$	$0.338\,502\,966 \times 10^{16}$	$-0.803\,004\,985 \times 10^{18}$	$0.732\,964\,756 \times 10^{20}$
$0 \to 9$	550	$0.106\,418\,750 \times 10^{-3}$	$-0.146\,917\,756 \times 10^{1}$	$0.289\,593\,294 \times 10^{5}$	$-0.336\,743\,387 \times 10^{7}$	$0.171\,303\,281 \times 10^{10}$	$0.173\,009\,739 \times 10^{13}$	$-0.296\,792\,983 \times 10^{16}$	$0.156\,774\,183 \times 10^{19}$	$-0.292\,893\,172 \times 10^{21}$
$0 \to 10$	600	$0.144\,300\,838 \times 10^{-4}$	$-0.135\,396\,575 \times 10^{1}$	$0.296\,834\,933 \times 10^{5}$	$0.806\,531\,715 \times 10^{7}$	$-0.280\,264\,726 \times 10^{11}$	$0.444\,214\,735 \times 10^{14}$	$-0.379\,357\,647 \times 10^{17}$	$0.167\,825\,913 \times 10^{20}$	$-0.301\,076\,067 \times 10^{22}$
$0 \to 11$	650	$0.867\,766\,831 \times 10^{-7}$	$-0.958\,697\,496 \times 10^{0}$	$0.257\,440\,709 \times 10^{5}$	$0.409\,137\,189 \times 10^{8}$	$-0.119\,011\,764 \times 10^{12}$	$0.189\,804\,083 \times 10^{15}$	$-0.170\,031\,924 \times 10^{18}$	$0.799\,092\,375 \times 10^{20}$	$-0.152\,981\,923 \times 10^{23}$
$0 \to 12$	700	$0.325\,017\,591 \times 10^{-32}$	$0.446\,113\,412 \times 10^{1}$	$-0.512\,283\,310 \times 10^{5}$	$0.493\,759\,852 \times 10^{9}$	$-0.147\,156\,377 \times 10^{13}$	$0.246\,380\,214 \times 10^{16}$	$-0.232\,988\,126 \times 10^{19}$	$0.115\,912\,196 \times 10^{22}$	$-0.235\,418\,187 \times 10^{24}$

Table 4. Parameters used in equation (18) to represent the VE and VdE rate coefficients of CO^+ ($v' = 1$).

$v' \to v''$	$T_{\min}$ (K)	$A_{v' \to v''}$	$\alpha_{v' \to v''}$	$B_{v' \to v''}(1)$	$B_{v' \to v''}(2)$	$B_{v' \to v''}(3)$	$B_{v' \to v''}(4)$	$B_{v' \to v''}(5)$	$B_{v' \to v''}(6)$	$B_{v' \to v''}(7)$
$1 \to 0$	100	$0.633\,920\,326 \times 10^{-5}$	$-0.770\,044\,378 \times 10^{0}$	$0.104\,178\,437 \times 10^{4}$	$-0.551\,232\,678 \times 10^{6}$	$0.175\,018\,067 \times 10^{9}$	$-0.374\,062\,491 \times 10^{11}$	$0.492\,117\,834 \times 10^{13}$	$-0.348\,198\,826 \times 10^{15}$	$0.100\,308\,337 \times 10^{17}$
$1 \to 2$	100	$0.112\,757\,539 \times 10^{-5}$	$-0.667\,253\,557 \times 10^{0}$	$0.301\,658\,328 \times 10^{4}$	$0.265\,128\,201 \times 10^{6}$	$-0.167\,485\,020 \times 10^{9}$	$0.460\,282\,036 \times 10^{11}$	$-0.652\,022\,601 \times 10^{13}$	$0.465\,696\,778 \times 10^{15}$	$-0.132\,656\,980 \times 10^{17}$
$1 \to 3$	150	$0.562\,989\,138 \times 10^{-6}$	$-0.651\,039\,420 \times 10^{0}$	$0.526\,482\,012 \times 10^{4}$	$0.134\,397\,812 \times 10^{7}$	$-0.848\,709\,209 \times 10^{9}$	$0.288\,214\,188 \times 10^{12}$	$-0.547\,449\,693 \times 10^{14}$	$0.544\,047\,009 \times 10^{16}$	$-0.219\,710\,957 \times 10^{18}$
$1 \to 4$	200	$0.130\,991\,873 \times 10^{-6}$	$-0.537\,069\,718 \times 10^{0}$	$0.875\,368\,149 \times 10^{4}$	$0.339\,794\,737 \times 10^{6}$	$-0.146\,345\,601 \times 10^{9}$	$0.270\,246\,030 \times 10^{11}$	$0.183\,890\,443 \times 10^{12}$	$-0.736\,617\,748 \times 10^{15}$	$0.699\,602\,764 \times 10^{17}$
$1 \to 5$	250	$0.209\,439\,988 \times 10^{-5}$	$-0.858\,043\,793 \times 10^{0}$	$0.147\,483\,446 \times 10^{5}$	$-0.617\,683\,461 \times 10^{7}$	$0.628\,994\,423 \times 10^{10}$	$-0.343\,234\,925 \times 10^{13}$	$0.103\,740\,710 \times 10^{16}$	$-0.163\,563\,141 \times 10^{18}$	$0.104\,899\,664 \times 10^{20}$
$1 \to 6$	300	$0.439\,087\,022 \times 10^{-5}$	$-0.950\,117\,793 \times 10^{0}$	$0.180\,805\,100 \times 10^{5}$	$-0.780\,708\,040 \times 10^{7}$	$0.975\,729\,438 \times 10^{10}$	$-0.654\,274\,154 \times 10^{13}$	$0.239\,495\,154 \times 10^{16}$	$-0.451\,595\,265 \times 10^{18}$	$0.342\,947\,398 \times 10^{20}$
$1 \to 7$	350	$0.990\,587\,644 \times 10^{-5}$	$-0.107\,079\,534 \times 10^{1}$	$0.209\,321\,916 \times 10^{5}$	$-0.904\,877\,766 \times 10^{7}$	$0.124\,117\,280 \times 10^{11}$	$-0.929\,195\,541 \times 10^{13}$	$0.387\,627\,434 \times 10^{16}$	$-0.844\,294\,279 \times 10^{18}$	$0.746\,823\,381 \times 10^{20}$
$1 \to 8$	400	$0.290\,364\,496 \times 10^{-5}$	$-0.976\,365\,340 \times 10^{0}$	$0.209\,545\,755 \times 10^{5}$	$0.435\,177\,075 \times 10^{7}$	$-0.136\,200\,658 \times 10^{11}$	$0.175\,763\,114 \times 10^{14}$	$-0.114\,936\,867 \times 10^{17}$	$0.372\,696\,383 \times 10^{19}$	$-0.475\,130\,034 \times 10^{21}$
$1 \to 9$	450	$0.553\,151\,534 \times 10^{-5}$	$-0.107\,588\,250 \times 10^{1}$	$0.228\,931\,552 \times 10^{5}$	$0.102\,630\,980 \times 10^{8}$	$-0.292\,944\,159 \times 10^{11}$	$0.393\,966\,744 \times 10^{14}$	$-0.277\,151\,718 \times 10^{17}$	$0.982\,366\,990 \times 10^{19}$	$-0.138\,325\,077 \times 10^{22}$
$1 \to 10$	500	$0.295\,872\,921 \times 10^{-18}$	$0.190\,367\,144 \times 10^{1}$	$-0.111\,794\,851 \times 10^{5}$	$0.184\,960\,763 \times 10^{9}$	$-0.439\,761\,036 \times 10^{12}$	$0.564\,818\,219 \times 10^{15}$	$-0.399\,526\,307 \times 10^{18}$	$0.146\,086\,706 \times 10^{21}$	$-0.215\,320\,891 \times 10^{23}$
$1 \to 11$	550	$0.860\,719\,793 \times 10^{-14}$	$0.818\,099\,637 \times 10^{0}$	$0.202\,216\,367 \times 10^{4}$	$0.144\,200\,890 \times 10^{9}$	$-0.371\,106\,005 \times 10^{12}$	$0.518\,902\,243 \times 10^{15}$	$-0.402\,326\,107 \times 10^{18}$	$0.162\,115\,803 \times 10^{21}$	$-0.264\,323\,393 \times 10^{23}$
$1 \to 12$	600	$0.238\,429\,782 \times 10^{-24}$	$0.309\,243\,990 \times 10^{1}$	$-0.287\,784\,203 \times 10^{5}$	$0.327\,916\,264 \times 10^{9}$	$-0.895\,346\,410 \times 10^{12}$	$0.135\,575\,406 \times 10^{16}$	$-0.114\,959\,696 \times 10^{19}$	$0.509\,491\,570 \times 10^{21}$	$-0.917\,135\,223 \times 10^{23}$
$1 \to 13$	650	$0.171\,475\,246 \times 10^{-53}$	$0.946\,512\,823 \times 10^{1}$	$-0.118\,535\,342 \times 10^{6}$	$0.845\,804\,438 \times 10^{9}$	$-0.241\,202\,045 \times 10^{13}$	$0.384\,508\,952 \times 10^{16}$	$-0.344\,818\,061 \times 10^{19}$	$0.162\,171\,803 \times 10^{22}$	$-0.310\,615\,978 \times 10^{24}$

Table 5. Parameters used in equation (18) to represent the VE and VdE rate coefficients of CO^+ ($v' = 2$).

$v' \to v''$	$T_{\min}$ (K)	$A_{v' \to v''}$	$\alpha_{v' \to v''}$	$B_{v' \to v''}(1)$	$B_{v' \to v''}(2)$	$B_{v' \to v''}(3)$	$B_{v' \to v''}(4)$	$B_{v' \to v''}(5)$	$B_{v' \to v''}(6)$	$B_{v' \to v''}(7)$
$2 \to 0$	100	$0.143\,264\,325 \times 10^{-5}$	$-0.676\,398$ 119×10^{0}	$0.770\,399$ 508×10^{3}	$-0.649\,235$ 829×10^{6}	$0.280\,763$ 127×10^{9}	$-0.687\,619$ 887×10^{11}	$0.943\,978$ 108×10^{13}	$-0.672\,803$ 202×10^{15}	$0.193\,189$ 057×10^{17}
$2 \to 1$	100	$0.110\,150\,559 \times 10^{-5}$	$-0.664\,642$ 895×10^{0}	$-0.475\,690$ 563×10^{2}	$0.274\,737$ 488×10^{6}	$-0.172\,309$ 109×10^{9}	$0.472\,936$ 617×10^{11}	$-0.669\,923$ 671×10^{13}	$0.478\,615$ 271×10^{15}	$-0.136\,383$ 154×10^{17}
$2 \to 3$	100	$0.296\,299\,450 \times 10^{-6}$	$-0.540\,421$ 763×10^{0}	$0.322\,902$ 717×10^{4}	$-0.185\,353$ 201×10^{6}	$0.102\,324$ 472×10^{9}	$-0.295\,771$ 623×10^{11}	$0.446\,770$ 807×10^{13}	$-0.336\,457$ 775×10^{15}	$0.998\,160$ 611×10^{16}
$2 \to 4$	150	$0.278\,155\,705 \times 10^{-5}$	$-0.783\,269$ 363×10^{0}	$0.680\,722$ 101×10^{4}	$-0.103\,878$ 379×10^{7}	$0.741\,843$ 999×10^{9}	$-0.276\,056$ 904×10^{12}	$0.549\,666$ 157×10^{14}	$-0.558\,745$ 281×10^{16}	$0.228\,035$ 409×10^{18}
$2 \to 5$	200	$0.266\,683\,567 \times 10^{-4}$	$-0.107\,862$ 034×10^{1}	$0.110\,175$ 934×10^{5}	$-0.322\,418$ 905×10^{7}	$0.245\,112$ 696×10^{10}	$-0.101\,947$ 642×10^{13}	$0.237\,960$ 237×10^{15}	$-0.292\,641$ 709×10^{17}	$0.147\,503$ 229×10^{19}
$2 \to 6$	250	$0.542\,147\,000 \times 10^{-5}$	$-0.983\,012$ 338×10^{0}	$0.122\,608$ 040×10^{5}	$0.321\,533$ 385×10^{6}	$-0.729\,487$ 979×10^{9}	$0.465\,646$ 557×10^{12}	$-0.147\,373$ 795×10^{15}	$0.236\,308$ 026×10^{17}	$-0.153\,015$ 638×10^{19}
$2 \to 7$	300	$0.317\,786\,833 \times 10^{-6}$	$-0.721\,222$ 477×10^{0}	$0.142\,487$ 517×10^{5}	$0.102\,722$ 134×10^{7}	$-0.582\,000$ 169×10^{9}	$0.484\,888$ 182×10^{11}	$0.644\,040$ 556×10^{14}	$-0.223\,384$ 907×10^{17}	$0.220\,068$ 495×10^{19}
$2 \to 8$	350	$0.273\,643\,357 \times 10^{-6}$	$-0.744\,726$ 391×10^{0}	$0.184\,645$ 633×10^{5}	$-0.445\,860$ 723×10^{7}	$0.783\,952$ 518×10^{10}	$-0.677\,237$ 281×10^{13}	$0.310\,300$ 559×10^{16}	$-0.723\,338$ 935×10^{18}	$0.674\,944$ 000×10^{20}
$2 \to 9$	400	$0.161\,814\,112 \times 10^{-5}$	$-0.947\,134$ 778×10^{0}	$0.222\,431$ 469×10^{5}	$-0.163\,473$ 342×10^{7}	$-0.438\,401$ 719×10^{10}	$0.980\,397$ 656×10^{13}	$-0.775\,362$ 755×10^{16}	$0.276\,484$ 946×10^{19}	$-0.372\,814$ 588×10^{21}
$2 \to 10$	450	$0.857\,949\,106 \times 10^{-5}$	$-0.113\,992$ 880×10^{1}	$0.247\,605$ 739×10^{5}	$0.513\,853$ 850×10^{7}	$-0.233\,874$ 625×10^{11}	$0.348\,626$ 787×10^{14}	$-0.254\,552$ 925×10^{17}	$0.917\,457$ 255×10^{19}	$-0.130\,303$ 783×10^{22}
$2 \to 11$	500	$0.222\,319\,239 \times 10^{-11}$	$0.337\,546$ 441×10^{0}	$0.802\,866$ 148×10^{4}	$0.966\,824$ 466×10^{8}	$-0.237\,713$ 634×10^{12}	$0.308\,999$ 968×10^{15}	$-0.219\,586$ 955×10^{18}	$0.804\,421$ 605×10^{20}	$-0.118\,654$ 044×10^{23}
$2 \to 12$	550	$0.967\,268\,411 \times 10^{-11}$	$0.141\,405$ 228×10^{0}	$0.108\,888$ 796×10^{5}	$0.100\,995$ 726×10^{9}	$-0.264\,030$ 143×10^{12}	$0.370\,381$ 461×10^{15}	$-0.287\,172$ 365×10^{18}	$0.115\,625$ 983×10^{21}	$-0.188\,366$ 916×10^{23}
$2 \to 13$	600	$0.859\,235\,026 \times 10^{-11}$	$0.675\,737$ 504×10^{-1}	$0.117\,098$ 302×10^{5}	$0.110\,881$ 879×10^{9}	$-0.305\,681$ 884×10^{12}	$0.463\,253$ 664×10^{15}	$-0.392\,591$ 768×10^{18}	$0.173\,889$ 056×10^{21}	$-0.312\,870$ 721×10^{23}
$2 \to 14$	650	$0.164\,458\,016 \times 10^{-23}$	$0.280\,896$ 167×10^{1}	$-0.257\,956$ 296×10^{5}	$0.332\,078$ 837×10^{9}	$-0.946\,887$ 885×10^{12}	$0.150\,871$ 571×10^{16}	$-0.135\,222$ 037×10^{19}	$0.635\,565$ 472×10^{21}	$-0.121\,648$ 562×10^{24}

measurements, probably due to the presence of $CO^+ \cdot (CO)_n$ clusters in the sample, as was pointed out by Whitaker *et al* (1981). Moreover, our calculations show a much smaller isotopic effect than was found by Guberman (2007), having a mean deviation of 0.43% (due to the different nuclear reduced masses) between the two isotopologues.

Finally, we have calculated dissociative recombination, and vibrational excitation (VE) and de-excitation (VdE) cross sections for different vibrational levels in the entrance channels, namely for $v_i^+ = 1$ and 2, and compared with the cross sections found for $v_i^+ = 0$. The comparison of the DR cross sections can be seen in figure 7. We find that the DR cross section for the ground vibrational levels exceeds significantly, by more than a factor of 2, those for $v_i^+ = 1$ and 2, whereas the latter have similar rates.

Figure 8 shows the total DR and vibrational transition (VE, VdE) rate coefficients for the three initial vibrational levels of the ion. We find the highest rates for all of the processes for $v_i^+ = 0$; their magnitude decreases with excitation of the initial ionic vibrational level, except for the $\Delta v = v_f^+ - v_i^+ = -1$ de-excitation transitions where $v_i^+ = 2$ gives higher rates. The trends of the observables are the same for the cross section and the rate coefficients. Thus one can conclude that whenever the initial sample can contain ions with excited vibrational levels, fully accounting for them will be important.

To aid the simple use of the rate coefficients shown in figure 8, we have fitted them using simple formulas. The calculated DR rate coefficients for CO^+ (v = 0, 1, 2) are represented by

$$k^{\mathrm{DR}}_{(\mathrm{CO}^+),v}(T_\mathrm{e}) = A_v T_\mathrm{e}^{\alpha_v} \exp\left[-\sum_{i=1}^{7} \frac{B_v(i)}{iT_\mathrm{e}^i}\right] \qquad (17)$$

over the electron temperature range $T_{\min} < T_\mathrm{e} < 5000$ K with $T_{\min} = 100$ K. The values given by equation (17) depart from the reference values by only a few per cent. The parameters A_v, α_v and $B_v(i)$ are listed in table 2. The corresponding formula for the vibrational transitions (VE and VdE) has the form

$$k^{\mathrm{VE,VdE}}_{(\mathrm{CO}^+),v'\to v''}(T_\mathrm{e}) = A_{v'\to v''} T_\mathrm{e}^{\alpha_{v'\to v''}} \exp\left[-\sum_{i=1}^{7} \frac{B_{v'\to v''}(i)}{iT_\mathrm{e}^i}\right] \qquad (18)$$

over the electron temperature range $T_{\min} < T_\mathrm{e} < 5000$ K. Again the values calculated using equation (18) depart from the reference values by only a few per cent. The parameters $T_{\min}$, $A_{v'\to v''}$, $\alpha_{v'\to v''}$, and the different $B_{v'\to v''}(i)$ for $i \in [1, 7]$ are listed in tables 3–5.

6. Conclusion

This paper presents a theoretical study of DR of CO^+ over a broad range of electron energies including several dissociation states with different symmetries. Although our basic approach is *ab initio*, using such methods it is not yet possible to compute the position of the dissociative curves involved in the DR process accurately enough to give reliable results. We have therefore used potential curves derived from spectroscopic data on CO to calibrate the *ab initio* data. Our DR calculations using these calibrated curves give good agreement with the experimental data for low energy, up to about 3 eV, significantly improving on the results of previous studies. We note however the very recent study of DR of N_2^+ performed by Little *et al* (2014) based on fully *ab initio* potential energy curves and couplings computed with the R-matrix method (Little and Tennyson 2013, Little and Tennyson 2014). N_2^+ is isoelectronic with CO^+, although its higher symmetry makes it somewhat easier to treat. These studies suggest that a similar, accurate, fully *ab initio* treatment of the CO^+ problem should be possible in the fairly near future.

A major motivation of this paper was to show and test the applicability of our method whenever there is a significant lack of reliable quantum chemistry calculations. We have performed calculations making use of four dissociation states in three different symmetries accounting for Rydberg states up to four partial waves. The calculations were done in the highest order of complexity possible.

Overall, one can say that the agreement achieved between theory and experiment over a significant range of energies is satisfactory, the trends being qualitatively reproduced for this diatomic system with many electrons. This suggests that our calibrated *ab initio* approach provides a suitable procedure for studying other many-electron systems for which pure *ab initio* calculations are not reliable.

The results presented are of fundamental importance and very promising, suggesting the need for further studies, especially with improved and more accurate potential energy curves, and couplings not just for the molecular ion but for the neutral molecule as well.

Acknowledgments

The authors thank Ch Jungen and S L Guberman for numerous and fruitful discussions. They acknowledge support from the International Atomic Energy Agency via the Coordinated Research Project 'Light Element Atom, Molecule and Radical Behaviour in the Divertor and Edge Plasma Regions', from Agence Nationale de la Recherche via the projects 'SUMOSTAI' (No. ANR-09-BLAN-020901) and 'HYDRIDES' (No. ANR-12-BS05-0011-01), from the IFRAF—Triangle de la Physique via the project 'SpecoRyd', and from the Centre National de la Recherche Scientifique via the programs 'Physique et Chimie du Milieu Interstellaire', and the PEPS projects 'Physique théorique et ses interfaces', TheMS and TPCECAM. They also acknowledge generous financial support from La Région Haute-Normandie via the CPER 'THETE' project, and the GRR Electronique, Energie et Matriaux, from the 'Fédération de Recherche Energie, Propulsion, Environnement', and from the LabEx EMC^3, via the project PicoLIBS (No. ANR-12-BS05-0011-01). KC thanks the Institut des Sciences de l'Ingénierie et des Systémes (INSIS) of CNRS for a research grant in 2013, and the Laboratoire Ondes et Matériaux Complexes (LOMC) of Le Havre University for hospitality.

References

Amitay Z *et al* 1999 *Phys. Rev.* A **60** 3769
Bultel A, Chéron B G, Bourdon A, Motapon O and Schneider I F 2006 *Phys. Plasmas* **13** 043502
Chakrabarti K and Tennyson J 2006 *J. Phys. B: At. Mol. Opt. Phys.* **39** 1485
Chakrabarti K and Tennyson J 2007 *J. Phys. B: At. Mol. Opt. Phys.* **40** 2135
Eidelsberg M *et al* 2012 *Astron. Astrophys.* **543** A69
Faure A and Tennyson J 2001 *Mon. Not. R. Astron. Soc.* **325** 443
Fowler A 1909 *Mon. Not. R. Astron. Soc.* **70** 176
Fox J L 1999 *Bull. Am. Astron. Soc.* **31** 5905
Fuente A, García-Burillo S, Gerin M, Rizzo J R, Usero A, Teyssier D, Roueff E and le Bourlot J 2010 *Astrophys. J.* **641** L105
Geoghegan M, Adams N G and Smith D 1991 *J. Phys. B: At. Mol. Opt. Phys.* **24** 2589
Giusti-Suzor A 1980 *J. Phys. B: At. Mol. Phys.* **13** 3867
Giusti-Suzor A, Bardsley J N and Derkits C 1983 *Phys. Rev.* A **28** 682-691
Greene C H and Jungen Ch 1985 *Adv. At. Mol. Phys.* **21** 51
Guberman S L 2000 *Dissociative Recombination: Theory, Experiment and Applications IV* M Larsson *et al* (Singapore: World Scientific) p 111
Guberman S L and Giusti-Suzor A 1991 *J. Chem. Phys.* **95** 2602
Guberman S L 2007 *Workshop on Planetary Atmospheres communication*
Jungen C 1996 *Molecular Applications of Quantum Defect Theory* (Bristol: IOP)
Jungen C and Atabek O 1977 *J. Chem. Phys.* **66** 5584
Kokoouline V, Greene C H and Esry B D 2001 *Nature* **412** 891
Kokoouline V and Greene C H 2003 *Phys. Rev.* A **68** 012703
Krupente P H and Weissman S 1965 *J. Chem. Phys.* **43** 1529
Laubé S, Lehfaoui L, Rowe B R and Mitchell J B A 1998 *J. Phys. B: At. Mol. Opt. Phys.* **31** 4181
Lefebvre-Brion H, Liebermann H P and Vázquez G J 2010 *J. Chem. Phys.* **132** 024311
Lefebvre-Brion H and Lewis B R 2007 *Mol. Phys.* **105** 1625
Little D A and Tennyson J 2013 *J. Phys. B: At. Mol. Opt. Phys.* **46** 145102
Little D A and Tennyson J 2014a *J. Phys. B: At. Mol. Opt. Phys.* **47** 105204
Little D A, Chakrabarti K, Mezei J Zs, Schneider I F and Tennyson J 2014b *Phys. Rev.* A **90** 052705
Mitchell J B A and Hus H 1985 *J. Phys. B: At. Mol. Phys.* **18** 547
Mentzoni M H and Donohoe J 1968 *Phys. Lett.* A **26** 330
Motapon O, Fifirig M, Florescu A, Waffeu Tamo F O, Crumeyrolle O, Varin-Bréant G, Bultel A, Vervisch P, Tennyson J and Schneider I F 2006 *Plasma Sources Sci. Technol.* **15** 23
Ngassam V, Motapon O, Florescu A, Pichl L, Schneider I F and Suzor-Weiner A 2003a *Phys. Rev.* A **68** 032704
Ngassam V, Florescu A, Pichl L, Schneider I F, Motapon O and Suzor-Weiner A 2003b *Eur. Phys. J.* D **26** 165
Park C *et al* 1994 *J. Thermophys. Heat Transfer* **8** 9
Pichl L, Nakamura H and Horacek J 2000 *Comput. Phys. Commun.* **124** 1
Rosen S, Peverall R, Larson M, Le Padellec A, Semaniak J, Larson Å , Strömholm C, van der Zande W J, Danared H and Dunn G H 1998 *Phys. Rev.* A **57** 4462
Schneider I F, Strömholm C, Carata L, Urbain X, Larsson M and Suzor-Weiner A 1997 *J. Phys. B: At. Mol. Opt. Phys.* **30** 2687
Schneider I F, Dulieu O and Giusti-Suzor A 1991 *J. Phys. B: At. Mol. Opt. Phys.* **24** L289
Schneider I F, Rabadán I, Carata L, Andersen L H, Suzor-Weiner A and Tennyson J 2000a *J. Phys. B: At. Mol. Opt. Phys.* **33** 4849
Schneider I F, Orel A E and Suzor-Weiner A 2000b *Phys. Rev. Lett.* **85** 3785
Seaton M J 1966 *Proc. Phys. Soc.* **88** 801
Seaton M J 1983 *Rep. Prog. Phys.* **46** 167
Sidis V and Lefebvre-Brion H 1971 *J. Phys. B: At. Mol. Phys.* **4** 1040
Sun H and Nakamura H 1990 *J. Chem. Phys.* **93** 6491
Takagi H 1993 *J. Phys. B: At. Mol. Opt. Phys.* **26** 4815
Takagi H 2000 *Dissociative Recombination: Theory, Experiment and Applications IV* ed M Larsson *et al* (Singapore: World Scientific) p 180
Tanabe T *et al* 1995 *Phys. Rev. Lett.* **75** 1066
Tchang-Brillet W-Ü L, Julienne P S, Robbe J-M, Letzeltel C and Rostas F 1992 *J. Chem. Phys.* **96** 6735
Tennyson J 1996a *J. Phys. B: At. Mol. Opt. Phys.* **29** 1817
Tennyson J 1996b *J. Phys. B: At. Mol. Opt. Phys.* **29** 6185
Vâlcu B, Schneider I F, Raoult M, Strömholm C, Larsson M and Suzor-Weiner A 1998 *Eur. Phys. J.* D **1** 71
Vázquez G J, Amero J M, Liebermann H P and Lefebvre-Brion H 2009 *J. Chem. Phys.* **113** 13395
Whitaker M, Biondi M A and Johnsen R 1981 *Phys. Rev.* A **23** 1481
Wigner E and Witmer E E 1928 *Z. Phys.* **51** 859